UNIVERSITY OF CALIFORNIA,

IRVINE

Joining Blood and Ferric Chloride in a Microfluidic Device

THESIS

Submitted in partial satisfaction of the requirements

for the degree of

MASTER OF SCIENCE

In Biomedical Engineering

by

Krystopher Lawrence

Thesis Committee:

Abraham Lee, Chair

Michelle Digman

Wendy Liu

2020

Contents

Chapter 1

1.1 Problem Statement

Venous thromboembolism is when pathological blood clotting occurs within the veins. These can most commonly occur in the legs, though deep veins elsewhere in the body, particularly the arms and brain, can be sites of embolism formation (1). Deep vein thrombosis in the legs can present symptoms such as swelling, redness, tenderness (1), and pain (2). When the embolism ends up in the lungs, it is called pulmonary embolism, and may cause symptoms such as difficulty breathing, chest pain, dizziness, rapid heartbeat, hyperventilation, and even coughing up blood (1). Pulmonary embolism following a stroke is possible, but according to literature is not commonly observed (2). However, patients who experienced acute stroke can still die of sudden death due to pulmonary embolism (2). Patients with less mobility, such as limb paralysis, are more likely to experience venous thromboembolism following stroke

versus patients with higher mobility (3). A proportion, about one in six, of all strokes are cardioembolic, meaning that the thrombus forms in the heart, such as in the myocardium, the left ventricle, or the mitral valve (4). As of the 1980s, a lack of validated diagnostic criteria and co-occurrence of atherosclerosis in the brain made it difficult to confirm a case of cardioembolism.

Venous thromboembolism, once discovered by imaging, is treated with anticoagulants. Heparin, whether in the low-molecular weight or unfractionated form, is a common choice (1). The former can be dosed based on weight without having to monitor activated partial thromboelastin time results, a routine coagulation screening test (1). However, unfractionated heparin is reversible with protamine and has a shorter half-life, making it more ideal for patients also receiving thrombolysis treatment (1). Patients without full renal function can also benefit from unfractionated heparin because clearance of the low-molecular-weight heparin may be inefficient and lead to accumulation in the body (1). If complications with heparin occur, there are non-oral alternatives which include fondaparinux, argatroban, and lepirudin (1). There are three stages of treatment: an acute stage in the days and up to a couple weeks following the embolism, a maintenance period of a few months during which the patient should also rest, and a longer term extended period of treatment (1).

A 2005 study on cardiovascular events following acute pulmonary embolism separated the patients into two groups: those who experienced an idiopathic venous thromboembolism and those who had transient risk factors, which would be if the embolism occurred following trauma, surgery, pregnancy, the use of oral contraceptives, or more than a week of immobilization (5). Patients with a first episode of pulmonary embolism had higher rates of arterial and venous incidents within 3 years, and these cardiovascular events were also the most common cause of death for these patients (5). Idiopathic pulmonary embolism showed more cardiovascular events than in pulmonary embolism with transient risk factors (5). The latter group did not even present arterial events. Most cardiovascular events occurred after treatment with anticoagulants, but prolonging oral anticoagulant use increases the risk for bleeding complications and needs to be monitored (5). The secondary venous events for idiopathic pulmonary

embolism were most often another pulmonary embolism (5). In general, anticoagulants are known not to work for preventing embolism in all patients, and between 5 and 45% of patients still experience cardiovascular events after treatment (6).

Deep vein thrombosis and pulmonary embolism are a major disease burden treated mainly by direct oral anticoagulants (1). There are 10 million cases of venous thromboembolism around the world per year, and the economic burden of this disease in the United States alone is estimated to be up to $10 billion (22). As imaging and detection methods improve, alongside an aging population and increase in comorbid conditions such as obesity, heart failure and cancer, incident rate is also increasing (1). The morbidity rate is high, with 20% of patients with pulmonary embolism who die within 30 days of diagnosis, and 30% of patients have a recurring instance within 10 years (1).

1.2 Proposed solution

Microfluidics can provide inexpensive and easily reproducible platforms for experiments involving hematologic and microvascular processes (7). The main advantage to microfluidics is the tight control of a dynamic fluidic environment on the microscale (7). Whereas parallel flow chambers, the previous technology, would need liters of blood to run a high shear experiment, an experiment of that time and length scale only needs microliters per minute for high shear in a microfluidic device (20). The 2014 study with Li et al could control a range of initial shear rates from 500 to 10,000 s^{-1} to demonstrate that thrombi formed at higher shear rates were more likely to detach and therefore embolize (6). These are helpful ranges because venous shear rates are around 100 to 200 s^{-1}, arterial shear rates are 1,000 to 2,000 s^{-1}, and pathological shear rates range from 10,000 up to 100,000 s^{-1} (8). Adhesion of platelets to coagulation factors, for example VWF (von Willebrand Factor), can be dependent on shear (8).

Experimentation with microfluidic devices also allow for tight control over biochemistry and channel geometry in a clotting system for copying the conditions in diseases of interest (20). Venous blood clots are rich in fibrin, while arterial blood clots are rich in platelets (9). This was shown to be

because fibrin deposition decreases with increasing shear rate (9). A microfluidic device with perpendicular cross-flows of thrombin and fibrinogen helped demonstrate how hemodynamics affect the fibrin assembly process (9). Shear rate was variable by simply varying the height, and thereby the inlet pressure, of the media above the thrombin channel relative to the fibrinogen channel (9). Flux of thrombin through the membrane separating its channel from the fibrinogen channel was then reported to change with changing shear rate (9). In the Muthard et al paper, initial shear wall stress was set by the flow rate of the upstream pump (10).

In microfluidics, it is also easy to see spatiotemporal changes in the structure and composition of clots using fluorescence microscopy since microfluidic devices are typically fabricated with transparent material (20). The small volumes of blood at this scale still have enough platelets and coagulation factors for statistically significant results (20).

The rectangular shape of typical microfluidic channels can interrupt flow patterns when trying to emulate physiological conditions, however (20). To get around this, some groups use a cylindrical material that can be removed later for PDMS to cure around, such as an optical fiber (20). The fiber could then create a stenosed region by being notched by a razor blade with sandpaper wrapped on the blade (20).

The low Reynolds number of the flow in microfluidic devices is a limitation, though. Higher Reynolds numbers are found in pathological flows of arterial stenosis, so the recirculation vortex distal of such a stenosis would be impossible in a microfluidic device under regular creeping flow (20). My lab's LCAT system could create vortices, but they would be produced by acoustic transduction instead of the flow in the device. The vortices would have to be known and controlled with acoustic frequency instead of being a studied variable.

Chapter 2 Background

The ferric chloride thrombosis model in mice consists of placing a small piece of paper that has been soaked in $FeCl_3$ aqueous solution onto the exposed carotid artery of a mouse. Kurz et al were the first to develop this model, but in rats, and had based it on an electrically induced injury model that worked only with iron-containing electrodes. The paper applied to the artery had been dipped in solutions varying from 5 to 65% $FeCl_3$ and a temperature probe would indicate when the artery became occluded. Time to occlusion was the varying parameter measured as a result of applying different concentrations of ferric chloride. Sixty minutes was the maximum time given for the vessel to occlude, so if it didn't occlude, 60 minutes was taken as the result. Time to occlusion decreased with increased ferric chloride concentration. The 50% ferric chloride solution application was difficult to be inhibited by heparin, so the researchers selected 35% as the preferred concentration for future studies, with a time to occlusion between 20 and 25 minutes. After 10 minutes of application, the luminal surface was observed to be stripped of endothelial cells and covered with adhered platelets and a few red and white blood cells mixed in. Then by about 20 minutes, an occlusive thrombosis with platelets, fibrin, and erythrocytes would be present. (11)

Endothelial cells are found to be removed by $FeCl_3$ applied to the exterior of the vessel. It used to be thought that this damage to the vessel would initiate thrombosis. However, the inner layers of the vessel are not exposed, so only basement membrane components could have contributed to thrombus formation (14). What appears to be a denuded endothelial surface might actually be remnants of red blood cells transiently adhering to the endothelium (15). One paper observed that "ferric ion-filled spherical bodies" appear on the endothelial cells which platelets then adhere to and form aggregates (14). Another found that platelets do not adhere directly to the endothelium but mostly to erythrocytes that have firmly adhered to the endothelium (15). Platelets adhered to these red blood cells then initiate thrombosis (15). By testing in scenarios with deficiencies of von Willebrand factor and GPIb-alpha, the paper demonstrated that neither is required for $FeCl_3$-induced erythrocyte adhesion. The VWF deficiency

resulted in a slower rate of thrombus formation, but the thrombosis still occurred because platelet recruitment could still occur, but merely slowed down (15). GPIb-alpha deficiency also slows the binding between platelets and erythrocytes, as it is a receptor on the platelets (15).

Most animal models use ferric chloride or laser activity to damage the vessel with free radicals and cause thrombosis even in non-murine animal models (18). Intraluminal injury is another method by which the vessel is opened and mechanically scratched to remove the intima, exposing collagen and other extracellular matrix components to the platelets and clotting factors to start thrombosis (18). Electrolytic injury applied to the arterial surface makes for a newer mouse model, and newer ones are being discovered but have not yet been standardized (18). Thrombosis is not just blood clotting, however, it is pathological blood clotting within a blood vessel without there being injury or bleeding that would necessitate a clot for hemostasis (18).

Thrombosis models on the veins are most useful for research relating to deep vein thrombosis, but mouse veins are fragile and have varying anatomy concerning their branches (18). Nevertheless, mouse vein-based thrombosis models have still helped confirm the effects of low flow in valve pockets, genetic risk factors that are orthologs in humans, and microvesicles (18), as well as elucidating the role of inflammatory cells in venous thrombosis (18). Zebrafish can also be studied for hemostasis and thrombus formation because they share ortholog genes with humans for coagulation, anticoagulation, and platelet signaling proteins (18). The same ferric chloride and laser activity models exist but are performed on zebrafish larvae only days after fertilization (18). The larvae are immobilized in agarose and then coated in ferric chloride or phenylhydrazine to induce thrombosis in the thin tail (18). Again, time to occlusion is the main way to measure an output parameter (18). The laser-induced model in zebrafish results in a half-moon structure that extends from the endothelium to the lumen of the vessel, with thrombocyte presence verified by antibody staining (18). Meanwhile, the ferric chloride model results in fibrin forming in clusters within the vessel (18). These animal models are limited in terms of mechanisms being poorly understood and poorly resembling actual pathological processes. The main advantage of these models is

that the roles of individual components can be studied through genetic knockdowns or through functional inactivation. Multiple models are still needed in the process of testing a new antithrombotic drug for humans (18).

Blood vessels in the human body range from 1 to 3 cm in the aorta down to 3 to 10 μm in the capillaries (19). Photolithography techniques for fabricating microfluidic devices can create features as small as 100nm (19), depending on the technique and skill of the handler. Adhesion of platelets onto denuded vessel walls is shear-dependent and highly regulated by complex flow, which can be studied easily in microfluidics (19). Under arterial flow conditions, von Willebrand Factor (VWF) is important for thrombus formation, while fibronectin and fibrinogen are more important at the lower, venous shears (19). VWF and fibrinogen form important substrates for clot formation in various prosthetics, including left ventricular assist devices (19). VWF captures platelet receptor GPIba in a transient shear-dependent interaction best studied under flow (19). There already exist microfluidic devices for measuring bleeding risk, particularly one which can monitor multiple output parameters including immobilized platelet number and aggregate morphology (19). Flow devices have been used to evaluate von Willebrand Disease, which is a deficiency in VWF and hemostasis, with varying linear shear rates and comparing clotting at the wall under a physiological blood flow (19).

For studying thrombosis in pathological blood flows, microfluidics are easy to use with good versatility, appropriate scale, and decent control of fluid conditions (20). The transparency of the devices is ideal for observation of spatiotemporal changes in clot structure and composition under a fluorescent microscope (20). Antibodies against blood components can be used to fluorescently track thrombosis (20). High shear experiments in microfluidics need far less blood than the previous technology of parallel flow chambers: microliters per minute versus liters of blood for the same time and length scale (20).

The platform in our lab can produce vascularized micro-organs that are perfused by physiological flow and contains tissue chambers with which extracellular matrix and cells are loaded (21). Cancer cell studies have traditionally been performed in 2D monoloayers, which ignore the extracellular matrix,

stromal cells, and vasculature of a tumor which have normally important functions *in vivo* in 3D (21). Experiments in the field with tumor spheroids address some of those problems but they lack vasculature, and the highly invasive tumor cells do not readily form spheroids, thus the tumor spheroid is inappropriate for some cancer cell types (21). By culturing human colorectal cancer or breast cancer with stromal cells and endothelial cells, a vascular network is formed within a week, and the tumor cells form small spheroids within and around the microvessels, like a tumor *in vivo* (21). Then drugs focus on either the vasculature itself or the glycolytic metabolism of the tumor cells (21). The platform proves itself to be simple and effective for microtumor growth and drug testing, not requiring external pumps, tubing, or robotics, and supportive of non-spheroidal tumor types (21).

Chapter 3 Methods and Experimental Design

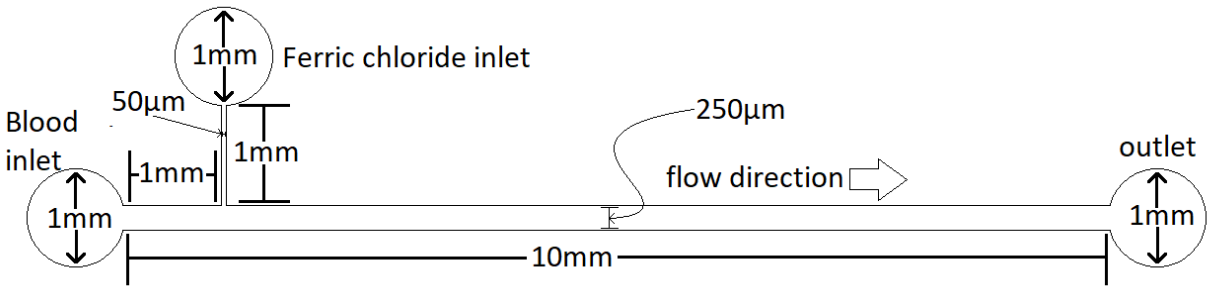

Figure 1 *The first design*

The above design was produced in AutoCAD based on the microfluidic device used in Ciciliano et al (16). The goal of this design is to flow blood from left to right, meeting the ferric chloride at the T-junction to theoretically produce clots. High pressure on the inlet will drive flow towards low pressure on the outlet. The main channel, for the flow of whole blood, is 250µm wide and 1cm long, while the side channel is 50µm wide and 1mm long, situated 1mm downstream from the edge of inlet pore on the far left. Aqueous $FeCl_3$ solution is to be added to the side channel at 5, 50, and 500mM concentrations. These concentrations were selected because Ciciliano et al had used 50mM $FeCl_3$ in their experiments with a similar design. Each inlet and outlet pore is 1mm in diameter and intended to

be used with an 18-gauge needle at the end of the tubing from a syringe pump. When the main channel is coated with endothelial cells, this T-junction reproduces the interface between endothelium, blood, and $FeCl_3$ as in the mouse model in which a small piece of paper soaked in ferric chloride is placed on a blood vessel to induce clotting (16).

Reynolds number in a channel is determined by the following equation,

$$Re = \frac{\rho v L}{\mu}$$

Where ρ is the density of the blood (1060 kg/m^3), v is the velocity of the blood (1.33×10^{-3} m/s for 1μL/min in the main channel), L is the characteristic length of the channel, and μ is the viscosity of the blood (taken to be about 3.5×10^{-3} Pa s). The characteristic length L was calculated as follows:

$$L = \frac{2ab}{a+b} = \frac{2 \cdot 250\mu m \cdot 50\mu m}{250\mu m + 50\mu m} = 8.33 \times 10^{-5} m$$

Where a and b are the width and height of the channel. The characteristic length is derived from the volume of the channel being divided by the surface area of the channel. The resulting Reynolds number is 0.0337, confirming laminar flow. The $FeCl_3$ solution will meet whole blood at the intersection and continue along the channel wall on the same side as the side channel since flow in the channel at 1μL/min will be in an orderly fashion, with each layer of molecules traveling in parallel lines toward the outlet. Since the initial concentration of $FeCl_3$ in the main channel will be 0mM, the incoming $FeCl_3$ from the side channel will diffuse throughout the main channel due to the concentration gradient, as well as the incoming convection.

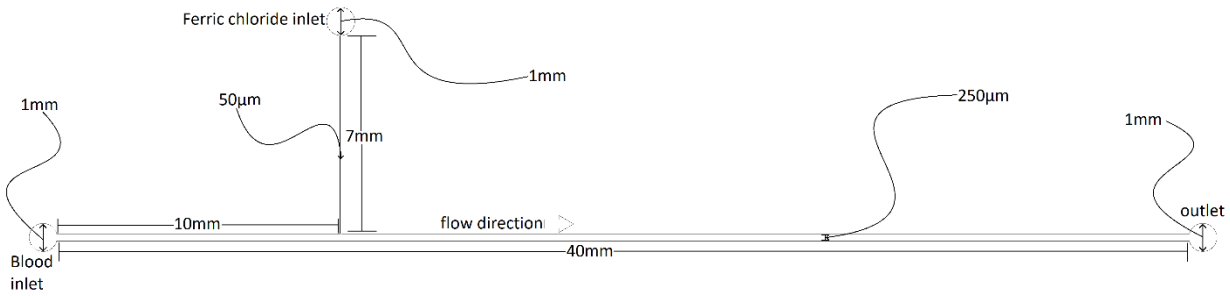

Figure 2 *The second design*

Our lab more often depends on hydrostatic flow to move fluid through our devices. A second design was made in AutoCAD to accommodate for the 1cm diameter of the Nalgene vials, which would be placed over the 1mm pores. The main channel was lengthened to 4cm, the side channel to 7mm, and the side channel was displaced to 1cm away from the edge of the inlet pore on the far left. The widths of the channel remained the same.

The mold to produce devices was fabricated with SU-8 2050 negative photoresist on a 3-inch silicon wafer via photolithography. For photolithography, the silicon wafer was first rinsed by deionized water and air-dried with a nitrogen gun. Then, the remaining moisture was evaporated off in the 65C oven for approximately two minutes. The wafer was then put in the Laurell spinner for 30s on 500rpm with an acceleration of 100rpm/s and then for 20s at 3250rpm to achieve a thickness of 50um of SU-8 2050 on the wafer. The soft bake step was performed at 65C and then 95C. The wafer was exposed to UV light for 16 seconds and returned to the two ovens for post-exposure bake. After development in a sonicated bath with SU-8 developer, the wafer was rinsed with IPA and dried with the nitrogen gun.

Next, single layer devices were poured from 10:1 PDMS basement to cross-linker by mass. For example, if a mold required 20g of PDMS, 18.2g basement plus 1.8g cross-linker would be utilized to equal 20g. In practice, 22.7g of basement was added to 2.3g of cross-linker in order to ensure that there was at least 20g of PDMS to pour out of the weighing boat. 20g of basement plus 2g of cross-linker could alternatively be used.

Uncured PDMS was then degassed in a vacuum chamber until air bubbles were minimized, on average for 20 to 40 minutes depending on the amount of PDMS degassed at a time. The PDMS was then poured onto a mold etched onto a 3-inch silicon wafer in an 8cm diameter polystyrene dish.

The PDMS cured at room temperature on a level surface overnight (18h). In the morning, the mold was transferred to a 65C oven for approximately an hour to complete the curing process. Following removal from the mold, the devices were cut with a scalpel to a size of approximately 40

by 18mm to enable them to fit onto the 75mm by 25mm glass slides that they would be bonded to. The outlet and inlet pores were punched with a 1mm hole punch.

The device layer was plasma bonded to a 1mm sheet of manufactured PDMS that cut to a rectangular shape (40 by 20mm) that would accommodate for the size of the microfluidic design. Then the device was plasma bonded to a glass slide as a stable substrate. Plastic Nalgene vials with the bottoms cut off were "glued" to the inputs of the device using PDMS. Pipet tips inserted within the punched holes prevented uncured PDMS from filling the channel.

Differential volumes of blood and $FeCl_3$ solution were used to drive hydrostatic pressure and therefore flow in the devices. A volume of 500µL was used at each of the two inputs to produce high pressure, and a volume of 107µL was used at the output for low pressure. The main channel was expected to have a flow of nearly 4 µL/s with a pressure drop of about 52 Pa, as calculated from the following equation.

$$\Delta P = \frac{1}{2}\rho v^2$$

ΔP is the pressure drop across the channel, ρ is the density of the fluid in the channel, which is whole blood, and v is the velocity of the blood. This equation was derived from Bernoulli's principle although the channel is rectangular instead of a cylindrical tube.

Ferric chloride dissolved in HBSS at concentrations of 5, 50, and 500mM using the same volume of 500µL over the input hole. The narrower width of the $FeCl_3$ side channel ensured that resistance was greater and that flow in the side channel was lower compared to the main channel for the same pressure drop. Downstream, the channel was observed under the microscope for evidence of clotting until the channel potentially clotted completely. Time to first aggregation and to occlusion in seconds after introduction of ferric chloride were measured.

Chapter 4 Results

At first, the channel was primed with 8uL of $CaCl_2$ with the intent of achieving a final concentration of 0.05 M in the half a millimeter of blood that was anticipated to flow down the

channel. However, after four runs, the blood never traveled more than approximately 8mm in 72 hours along the 4cm-long channel, and therefore it did not reach the T-junction where the blood ought to meet the ferric chloride. Pictures of the blood's travel distance could not be taken under the microscope because of the shadow of the vial over the inlet. However, the ferric chloride solution at 500mM also did not flow within the time allotted. Calcium chloride is intended to recalcify sodium citrated blood so that it may regain the ability to clot, as described by Ciciliano et al (16). However, the blood available to our lab was EDTA-treated, therefore there was uncertainty regarding the effect of $CaCl_2$ for our available conditions.

For the second run, the channel was primed with blood instead of $CaCl_2$, however no significant difference was observed in flow after 72 hours. No clotting was observed, so the "blood priming" was not repeated for the third and fourth runs, performed simultaneously in a single device. After 12 hours, these third and fourth runs also did not demonstrate much flow into the channel. A texture check with a pipet tip revealed possible congealment of the blood, which no longer flowed within the vial as a fluid but moved around in soft and moist chunks when disturbed. With runs 2 through 4, the device was kept in a 37C incubator, whereas the first run was performed at room temperature. Run 4 was not primed with the calcium chloride, but the 8uL of $CaCl_2$ was placed and mixed into the input vial with 500uL of blood.

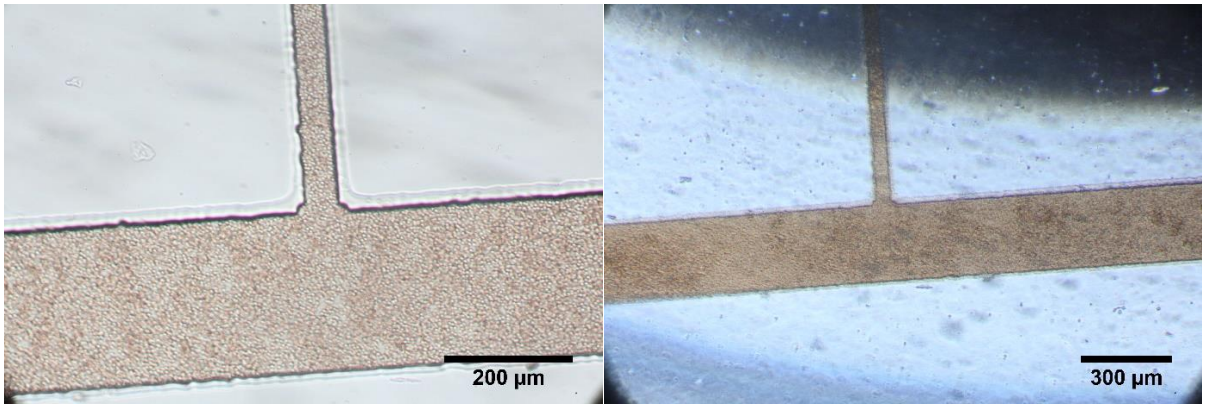

Figure 3: *Blood filling the channel in Run 2 before and after 72 hours. The channel was primed with blood and some agglomeration was observed, but frank clotting or a time to clot was not able to be identified. Flow is expected to have been negligible*.

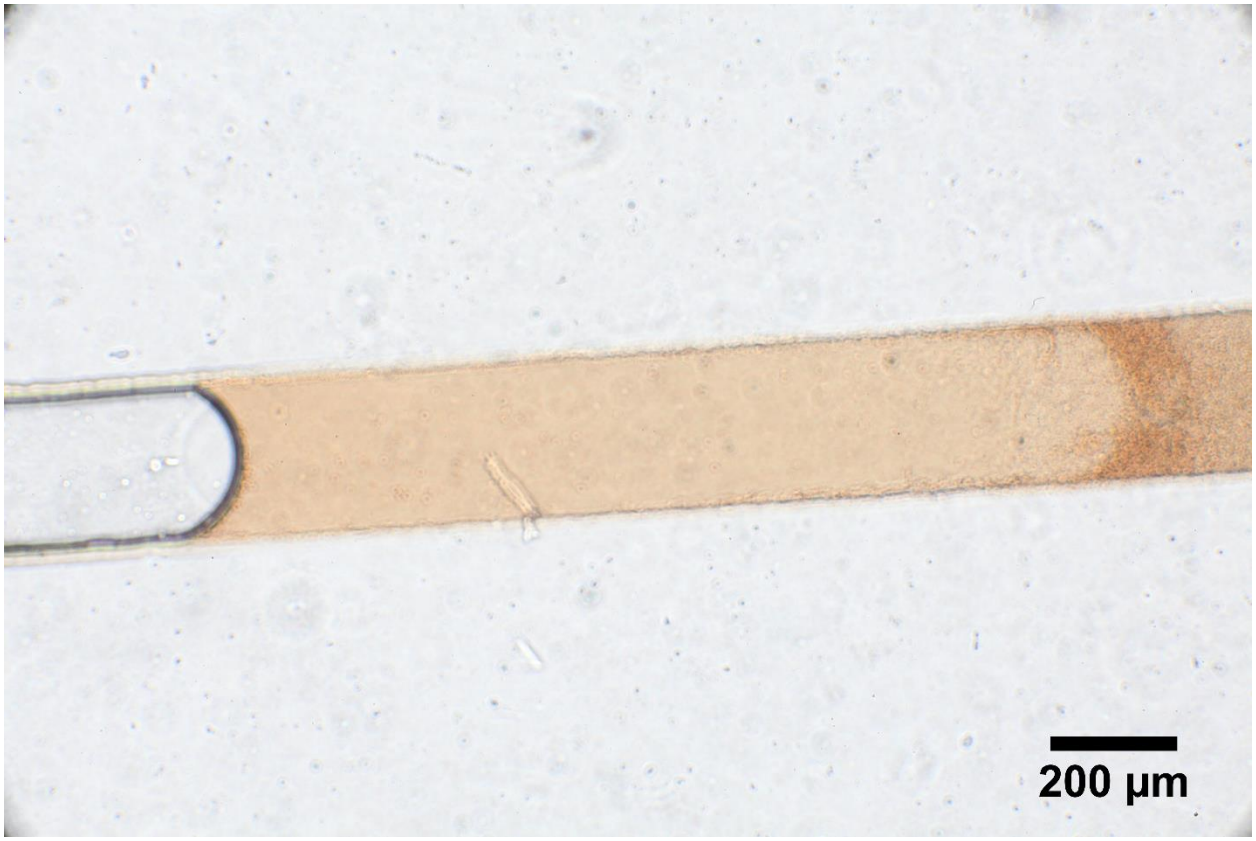

Figure 4: *T-junction is to the left; width of channel is 250um. In the second run, when the chamber was primed with blood, some of it receded and left a gas bubble in the center of the device around the T-junction. Some blood movement and agglomeration occurred here, although the exact nature of it is unknown.*

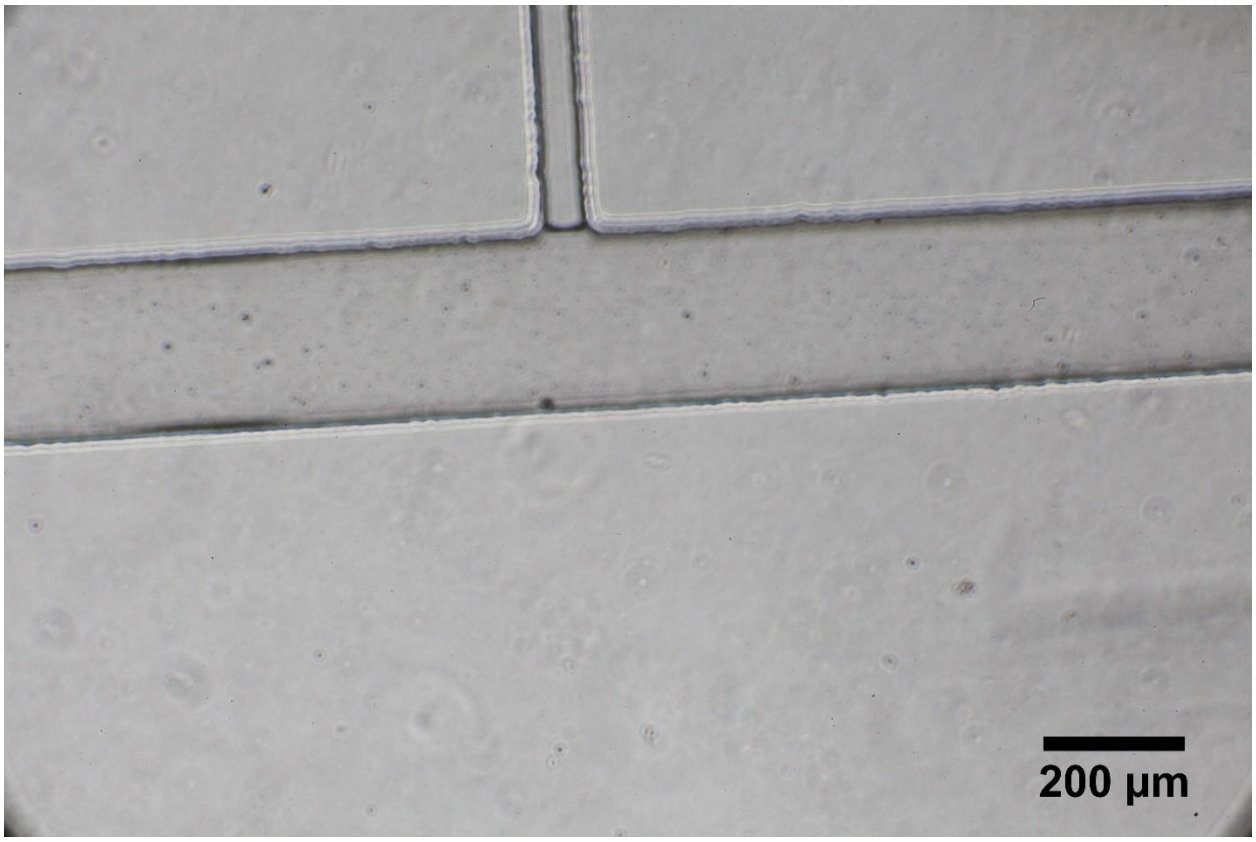

Figure 5: *Run 3 with $CaCl_2$ in the main channel. This fluid later evaporated over the course of the experiment*

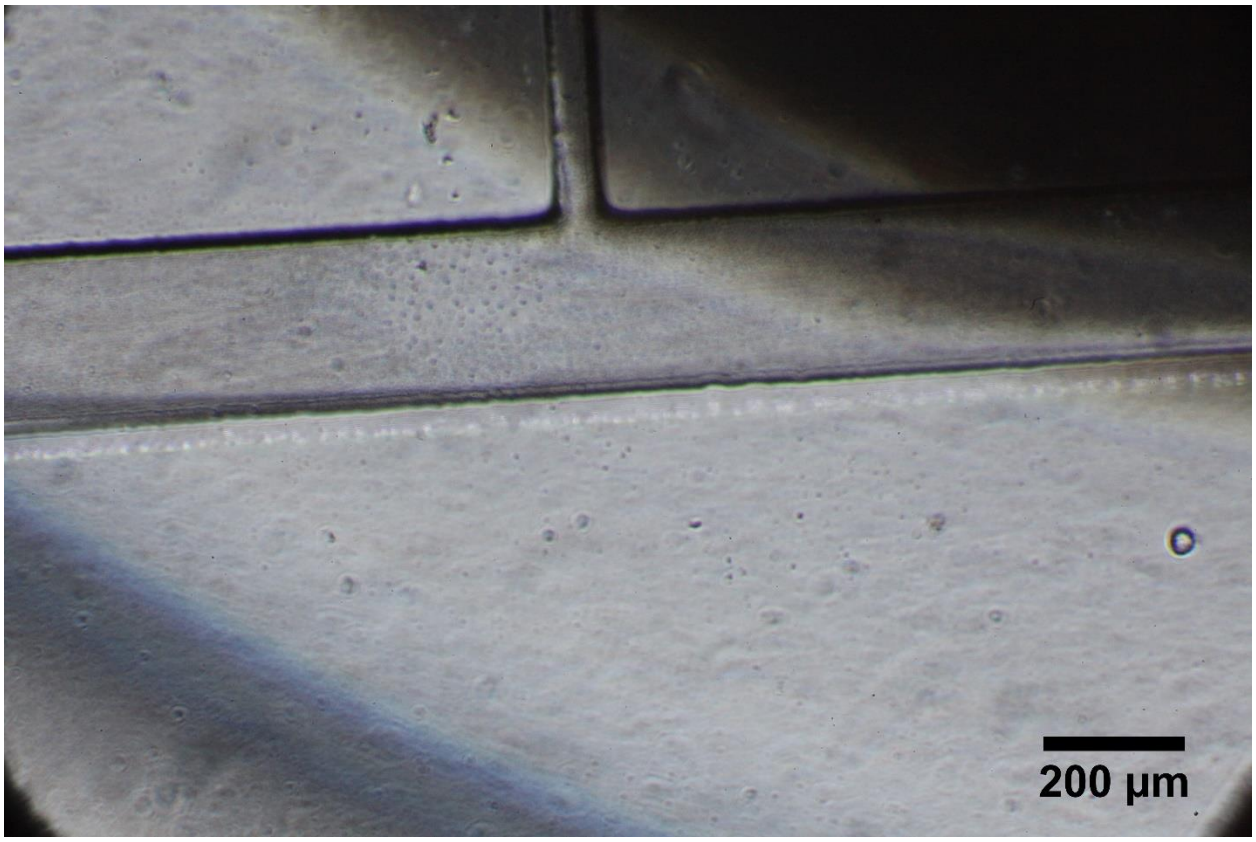

Figure 6**:** *Run 4 was not primed with CaCl2, and blood was able to travel within the main channel along a distance of approximately 5mm*

Chapter 5 Discussions

5.1 Alternate Plans

Hydrostatic vials do not work well for generating blood flow in a channel this size. A wider channel could decrease the resistance and therefore produce the pressure drop needed to let the fluid flow. The calculations for required pressure drop were inaccurate, as they used the Bernoulli equation, a poor estimation for flow through a rectangular channel. The following equation is normally used to estimate the pressure drop in a rectangular channel.

$$\Delta p = \frac{12\mu LQ}{wh^3}\frac{1}{\left[1-0{,}63\frac{h}{w}tanh\left(1{,}57\frac{w}{h}\right)\right]}$$

ΔP is the pressure drop across the channel, μ is the viscosity of the fluid within the channel, L is the length of the channel, Q is the flow rate of fluid in the channel, w is the width of the channel, and h is the height of the channel. This equation should produce a better estimate for the pressure drop required to achieve a desired flow rate, since now the dimensions of the channel are being considered. Lengthening the channel increases the resistance, and therefore increases the pressure drop required, while increasing the width and height of the channel decreases the resistance. However, according to this equation, 10300 Pa are required to achieve a flow rate of 1μL/min of blood in the main channel. The side channel would require 4720 Pa to flow $FeCl_3$ at the same speed. This amounts to nearly a meter of pressure head over the blood inlet and 46 cm of pressure head over the $FeCl_3$ inlet. These pressures cannot be achieved with the Nalgene vials that are only a few centimeters tall

Blood is a non-Newtonian fluid. Therefore, its viscosity is not constant and depends on the stress applied to it. At lower pressures, blood's viscosity is higher and requires a "yield stress" to initiate flow. Even more pressure may be required to initiate blood flow

A possible solution would be to use a syringe pump at 1-10μL/min. Since the device's main chamber holds less than a microliter, this speed is theorized to be enough to get blood cells visibly moving in the channel. Speeds of up to 60μL/min could be tested in the future with a syringe pump hooked up to the inputs of the device. The syringe can alternatively be hooked up to the outlet and drawn up, to pull fluid from both inlets into the main channel simultaneously.

Blood in this study was treated with EDTA as an anticoagulant. The ferric chloride paper used sodium citrated blood and recalcified it with $CaCl_2$ (16). EDTA also takes up the calcium and other metal ions in the blood that are critical for the coagulation cascade. Calcium chloride returns the calcium ions to the blood so that clotting is possible again. Although calcium chloride is expected to be used with citrated blood, it may still be able to enable clotting in EDTA-treated blood, too.

5.2 Future Directions

This project was pursued with the hope of generating blood clots to be passed on to our lab's vasculature-on-a-chip device. As tubing would be most ideal for connecting the blood clotting and vasculature devices, having a syringe pump setting the flow rate would be a better option than using hydrostatic vials. The device ought to be kept at 37C along with the tissue culture device growing vasculature on a chip. If exercise-on-a-chip can be developed in our lab, then this clotting device can be coupled with it to model deep vein thrombosis. The embolism would be produced in the clotting device, and then would pass through the channel and tubing until reaching the tissue culture device. The thrombus then may lodge within the vessels of the tissue culture device, blocking blood flow to part of the chamber. The exercise-on-a-chip device is planned to have oxygen control and pulsatile flow to model oxygen depletion and blood pressure changes from the heart's pulse.

My advisor informed me that molds in the lab usually have as many variations as possible on a single mask. A future mask could include the shorter design with closer inputs for syringe pump use. Channel lengths could be varied from 1 to 4cm for the main channel length, and 1 to 10mm for the side channel length. Applying negative pressure at the outlet is likely to be a more effective method to draw fluid into the main chamber from the two inlets. With that technique, hydrostatic vials will sit at the inputs for the blood and ferric chloride to produce high pressure, while the output has a syringe pump connected to pull at 1-10uL/min to create low pressure.

References

1- Di Niso, M., van Es, N., Büller, H. R. (2016) Deep vein thrombosis and pulmonary embolism. *The Lancet, 388*(10063), 3060-3073. doi: 10.1016/S0140-6736(16)30514-1

2- Wudicks, E.F.M. & Scott, J. P. (1997) Pulmonary embolism associated with acute stroke. *Mayo Clinic Proceedings, 72*(4), 297-300. doi: 10.4065/72.4.297

3- Colace, T.V., Muthard, R.W., Diamond, S.L. (2012) Thrombus growth and embolism on tissue factor-bearing collagen surfaces under flow: role of thrombin with and without fibrin. *Arterioscler Tromb Vasc Biol, 32*(6), 1466-1476. doi: 10.1161/ATVBAHA

4- Cardiogenic Brain Embolism: The Second Report of the Cerebral Embolism Task Force. (1989) *Arch Neurol, 46*(7), 727–743. doi:10.1001/archneur.1989.00520430021013

5- Becattini, C. et al. (2005) A prospective study on cardiovascular events after acute pulmonary embolism. *European Heart Journal, 26*(1), 77-83. doi: 10.1093/eurheartj/ehi018

6- Li, M., Hotaling, N.A., Ku D.N., Forest, C.R. (2014) Microfluidic thrombosis under multiple shear rates and antiplatelet therapy doses. *PLoS ONE, 9*(1), e82493. doi: 10.1371/journal.pone.0082493

7- Tsai, M., Kita, A., Leach J., Rounsevell, R., Huang, J.N., Moake, J., Ware, R.E., Fletcher, D.A., Lam, W.A. (2011) In vitro modeling of the microvascular occlusion and thrombosis that occur in hematologic diseases using microfluidic technology. *J Clin Invest, 122*(1), p408-418. doi: 10.1172/JCI58753

8- Colace, T.V., Tormoen, G.W., McCarty, O.J.T, Diamond, S.L. (2013) Microfluidics and coagulation biology. *Annual Review of Biomedical Engineering, 15*, p283-303. doi: 10.1146/annurev-bioeng-071812-152406

9- Welsh, J.D., Colace, T.V., Muthard, R.W., Stalker, T.J., Brass, L.F., Diamond, S.L. (2014) Platelet-targeting sensor reveals thrombin gradients within blood clots forming in microfluidic assays and in mouse. *J Thromb Haemost, 10*(11), p2344-2353. doi: 10.1111/j.1538-7836.2012.04928.x

10- Muthard, R.W., Diamond, S.L. (2013) Side view thrombosis microfluidic device with controllable wall shear rate and transthrombus pressure gradient. *Lab on a Chip, 13*(10), p.1883-1891. doi: 10.1039/C3LC41332B

11- Kurz, K.D., Main, B.W., Sandusky, G.E. (1990) Rat model of arterial thrombosis induced by ferric chloride. *Thromb Res, 60*(4), p269-280

12- Farrehi, P.M., Ozaki, C.K., Cameliet, P., Fay, W.P. (1998) Regulation of arterial thrombosis by plasminogen activator inhibitor-1 in mice. *Circulation, 97*(10), p1002-1008.

13- Wang, X., Smith, P.L., Hsu, M.Y., et al. (2006) Effects of factor XI deficiency on ferric chloride-induced vena cava thrombosis in mice. *J Thromb Haemost, 4*(9), p1982-1988.

14- Eckly, A., Hechler, B., Freund, M., et al. (2011) Mechanisms underlying $FeCl_3$-induced arterial thrombosis. *J Thromb Haemost, 9*(4), p779-789.

15- Barr, J.D., Chauhon, A.K, Schaeffer, G.V., Hansen, J.K., Motto, D.G. (2013) Red blood cells mediate the onset of thrombosis in the ferric chloride murine model. *Blood, 121*(18), p3633-3741.

16- Ciciliano, J.C., Sakurai, Y., Myers, D.R. et al. (2015) Resolving the multifaceted mechanisms of the ferric chloride thrombosis model using an interdisciplinary microfluidic approach. *Blood, 126*(6), p817-824.

17- Pandian, N.K.R., Mannino, R.G., Lam, W.A., Jain, A. (2018) Thrombosis-on-a-chip: Prospective impact of microphysiological models of vascular thrombosis. *Current Opinion in Biomedical Engineering, 5*, p29-34.

18- Jagadeeswaran, P., Cooley, B.C., Gross, P.L., Mackman, N. (2016) Animal models of thrombosis from zebrafish to nonhuman primates: Use in the elucidation of new pathologic pathways and the development of antithrombotic drugs. *Circulation Research, 118*(9), p1363-1379.

19- Zhang, C., Neelamegham, S. (2017) Application of microfluidic devices in studies of thrombosis and hemostasis. *Platelets, 28*(5), p434-440.

20- Herbig, B. A., Yu, X., & Diamond, S. L. (2018). Using microfluidic devices to study thrombosis in pathological blood flows. *Biomicrofluidics, 12*(4), 042201.

21- Sobrino, A., Phan, D.T.T, Datta, R., Wang, X., Hachey, S.J., Romero-Lopez, M., Gratton, E., Lee, A.P., George, S.C., Hughes, C.C.W. (2016) 3D microtumors in vitro supported by perfused vascular networks. *Scientific Reports, 6*(31589). DOI: 10.1038/srep31589.

22- Grosse, S.D., Nelson, R.E., Nyarko, K.A., Richardson, L.C., Raskob, G.E. (2016) The economic burden of incident venous thromboembolism in the United States: a review of estimated attributable healthcare costs. *Thromb Res, 137,* p3-10.